OXFORD

Cerebral Cortex, 2015, 1–16

doi: 10.1093/cercor/bhv082
Original Article

ORIGINAL ARTICLE

Exploring the Early Organization and Maturation of Linguistic Pathways in the Human Infant Brain

Jessica Dubois[1,2,3], Cyril Poupon[4], Bertrand Thirion[2,3,5], Hina Simonnet[1,2,3], Sofya Kulikova[6,7,8], François Leroy[1,2,3], Lucie Hertz-Pannier[6,7,8], and Ghislaine Dehaene-Lambertz[1,2,3]

[1]INSERM, U992, Cognitive Neuroimaging Unit, Gif-sur-Yvette, France, [2]CEA, NeuroSpin Center, Gif-sur-Yvette, France, [3]University Paris Sud, Orsay, France, [4]CEA, NeuroSpin Center, UNIRS, Gif-sur-Yvette, France, [5]INRIA, Parietal, Gif-sur-Yvette, France, [6]INSERM, U1129, Paris, France, [7]CEA, NeuroSpin Center, UNIACT, Gif-sur-Yvette, France, and [8]University Paris Descartes, Paris, France

Address correspondence to Jessica Dubois, PhD, CEA/SAC/DSV/I2BM/NeuroSpin/Cognitive Neuroimaging Unit U992, Bât 145, point courrier 156, 91191 Gif-sur-Yvette, France. Email: jessica.dubois@centraliens.net

Abstract

Linguistic processing is based on a close collaboration between temporal and frontal regions connected by two pathways: the "dorsal" and "ventral pathways" (assumed to support phonological and semantic processing, respectively, in adults). We investigated here the development of these pathways at the onset of language acquisition, during the first post-natal weeks, using cross-sectional diffusion imaging in 21 healthy infants (6–22 weeks of age) and 17 young adults. We compared the bundle organization and microstructure at these two ages using tractography and original clustering analyses of diffusion tensor imaging parameters. We observed structural similarities between both groups, especially concerning the dorsal/ventral pathway segregation and the arcuate fasciculus asymmetry. We further highlighted the developmental tempos of the linguistic bundles: The ventral pathway maturation was more advanced than the dorsal pathway maturation, but the latter catches up during the first post-natal months. Its fast development during this period might relate to the learning of speech cross-modal representations and to the first combinatorial analyses of the speech input.

Key words: brain development, diffusion imaging, interhemispheric asymmetry, language network, white matter maturation and myelination

Introduction

During the first post-natal year, infants rapidly learn the distribution of sounds used in their native language and the rules that govern the combination of these sounds into words (Jusczyk 1997). Although speech production lags behind perception, infants progressively improve their articulatory control to converge to a babbling that is specific to the native language between 6 months and 1 year of age (de Boysson-Bardies and Vihman 1991). They also rapidly integrate the auditory, visual, and motor aspects of speech in their efforts to imitate adults' utterances (Kuhl and Meltzoff 1982, 1996; Bristow et al. 2009). The neural bases of this sophisticated learning remain poorly understood, but the rise of noninvasive brain imaging techniques presents new opportunities to study early brain development in healthy human infants.

In adults, language perception and production rely on a large-scale network of cortical regions, generally lateralized toward the left hemisphere, and imply a close cooperation between the superior temporal, inferior parietal (angular and supramarginal gyri), and inferior frontal regions (pars opercularis and

triangularis; Price 2010; Pallier et al. 2011). The temporal regions have been classically considered to be involved in perception, whereas frontal regions are more concerned with the motor aspect of speech. This coarse distinction remains valid, although new models of language computation are more spatially distributed (Petersson et al. 2012). Postmortem descriptions, electrostimulation studies of epilepsy and tumor patients, and in vivo mappings that utilize diffusion imaging have isolated several white matter bundles that connect these brain regions and support language processing (Dick and Tremblay 2012). These bundles are divided into two pathways that superiorly and inferiorly surround the sylvian fissure: the dorsal pathway [arcuate fasciculus (AF) and superior longitudinal fasciculus (SLF)] and the ventral pathway [uncinate fasciculus (UF), inferior fronto-occipital fasciculus (iFOF), and fibers passing through the extreme capsule (EC), in between the claustrum and the external capsule], plus the inferior and middle longitudinal fascicles (ILF and MLF), which run within the temporal lobe. Although their respective contributions to different aspects of speech are still being discussed, the functions of these pathways are assumed to be markedly distinct: The "dorsal pathway" mainly contributes to phonological processing, whereas the "ventral pathway" supports semantic processing (Rolheiser et al. 2011; Dick and Tremblay 2012; Vandermosten et al. 2012).

The first functional MRI studies in infants listening to speech have reported activations that are very similar to those in adults. At 3 months of age, speech stimuli already activate temporal regions, more strongly in the left "planum temporale" than in its right counterpart (Dehaene-Lambertz et al. 2002, 2010). More surprisingly given the weak production capacities of infants and the commonly assumed delay in maturation of frontal regions, frontal activations have also been reported (Dehaene-Lambertz, Hertz-Pannier, et al. 2006; Perani et al. 2011). They are even observed before term, in 30-week gestational age preterm newborns who were studied in a syllable discrimination task using near-infrared spectroscopy (Mahmoudzadeh et al. 2013). In 3-month-old post-term infants, activations were enhanced in the left inferior frontal region when a short sentence was repeated, compared with trials when a new sentence was presented (Dehaene-Lambertz, Dehaene, et al. 2006). Because the delay between sentences was around 12 s, well above the capacity of the auditory sensory buffer, this result might suggest an already functional short-term verbal memory, which relies in adults on the dorsal linguistic pathway. Activations in orbito-frontal regions have also been observed during the first post-natal months, with different responses to a familiar (i.e., the mother) and unfamiliar (i.e., another mother) voice (Dehaene-Lambertz et al. 2010). These results challenge the classical assumptions that frontal regions and the connections to them are barely functional in the early post-natal months. However, these findings are congruent with a recent reappraisal of cortical maturation based on a structural MRI analysis of healthy infants, which has revealed that the maturation stages of the inferior frontal and planum temporale are similar and more advanced than those of more ventral regions, such as the superior temporal sulcus (STS; Leroy et al. 2011). Thus, the role of frontal regions in language learning should be reconsidered, and a better description of temporo-frontal connections might help to understand how the perisylvian network develops to efficiently process speech and adapts to the features of the native language.

In this cross-sectional study, diffusion imaging was used to explore the development of the main linguistic pathways in infants aged 6–22 weeks compared with adults. Our goal was two-fold. First, we investigated whether refined in vivo imaging techniques can highlight structural similarities between the infants' and adults' connectivity. Although histological examinations reported that the long axonal fibers between distant associative regions mainly grow during the second part of pregnancy (Huang et al. 2006; Vasung et al. 2010; Takahashi et al. 2012; Dubois et al. 2015), two previous in vivo studies in healthy newborns have reported that the AF ends in the premotor cortex, and that the branch terminating in Broca's area is not observed at this age (Perani et al. 2011; Brauer et al. 2013). However, in vivo fiber tractography in adults is subject to errors and approximations, and these errors may be even higher in infants due to the poor myelination and the small structure size, requiring anisotropy thresholds to be tuned for each group (Dubois et al. 2006; Dubois, Dehaene-Lambertz, Perrin, et al. 2008). It is thus a challenge to judge the bundles, functionality and similarity at different ages only based on tractography. We here proposed to complement this approach by a clustering analysis based on diffusion tensor imaging (DTI) parameters, and examine the similarities of these bundles between infants and adults in terms of terminations, asymmetry, and microstructure. Diffusivities and anisotropy are differently sensitive to the organization of the tracts (coherence, compactness, density, etc.; Dubois, Dehaene-Lambertz, Perrin, et al. 2008; Dubois, Dehaene-Lambertz, et al. 2014), and we expected these structural characteristics to be similar across ages, although possible differences in the tract terminations may be observed for the least mature regions. We further hypothesized equivalence among the two groups in terms of interhemispheric asymmetries, despite contradictory findings reported for the developing AF (Dubois et al. 2009; Song et al. 2014).

Our second goal was to investigate the between-bundles differences in maturation. White matter gets intensely myelinated during infancy and childhood, but the tempo of this myelination differs by brain region (Flechsig 1920; Yakovlev and Lecours 1967; Brody et al. 1987; Kinney et al. 1988). This asynchronous maturation can be indirectly followed in infants based on changes in DTI parameters (Dubois, Dehaene-Lambertz, Perrin, et al. 2008). For example, the acceleration of the visual P1 wave correlated with transverse diffusivity and anisotropy in the optic radiations (Dubois, Dehaene-Lambertz, Soares, et al. 2008), and several studies of older children and adults have highlighted correlations between performances in a cognitive task and the microstructural properties of tracts (e.g., reading capacities and DTI parameters in the AF; Thiebaut de Schotten et al. 2012). These results provide direct evidence of the relationships between DTI parameters and the pathways functional efficiency through myelination. In this study, we investigated the specific maturational tempos of language network bundles in infants. First, we analyzed differences in the bundle maturation over the whole group of babies, by considering DTI parameters normalized by the corresponding adult parameters to take into account intrinsic structural differences across bundles (Dubois, Dehaene-Lambertz, Perrin, et al. 2008). Then, we performed a cross-sectional analysis of age-related changes to examine whether specific trajectories were observed over this 16-week developmental period. We particularly focused on differences in the maturation of the dorsal and ventral pathways. To date, the role of the dorsal pathway in the first stages of language acquisition has been debated. Because of differences between the infants' and adults' AF tractography, some authors suggested that only the ventral pathway between Broca's area and temporal regions is functional during the first years of life, and account for the infant functional activations in the inferior frontal region (Perani et al. 2011; Brauer et al. 2013). Furthermore, the main hypothesis in evolutionary developmental biology claims that structures that appeared first during evolution

develop early on in contemporary organisms. Because the AF has evolved more recently than the EC/iFOF along the primate lineage (Rilling et al. 2008, 2012; Petrides and Pandya 2009), the ventral pathway is expected to mature earlier than the dorsal pathway. However, we suspected the fronto-temporal dorsal pathway to be efficient early during development because of functional evidence for verbal short-term memory capacities in infants (Dehaene-Lambertz, Hertz-Pannier, et al. 2006), and of correlations between indices of maturation in the AF, in Broca's region and in the posterior STS (i.e., in cortical regions that serve the phonological loop in adults) (Leroy et al. 2011). Furthermore, during the first post-natal trimester, infants' speech production increases qualitatively and quantitatively. When they imitate adults' models, vowel categories become more and more distinguishable (Kuhl and Meltzoff 1996). It suggests intense exchange (through connections of the dorsal pathway) between production centers in the inferior frontal region, and the phonological store in the posterior temporal region. Similarly, the first analyses of the speech distributional properties to discover reproducible relations between adjacent (Johnson and Tyler 2010) and non-adjacent syllables (Friederici et al. 2011) may benefit from an efficient short-term verbal memory, and thus a functional dorsal pathway.

Materials and Methods

Subjects

We studied 21 healthy infants (9 girls and 12 boys) born at term and with a mean age at MRI comprised between 5.9 and 22.4 weeks (chronological age corrected for gestational age at birth between 3.4 and 21 weeks). Seventeen young adults were also studied (7 women and 10 men; 20.8–27.4 years). The MRI protocol was approved by the regional ethical committee for biomedical research, and all parents and adult subjects gave written informed consents. Infants were spontaneously asleep during MR imaging. Particular precautions were taken to minimize noise exposure by using customized headphones and covering the magnet tunnel with a special noise protection foam.

Data Acquisition

Acquisitions were performed on a 3-T MRI system (Tim Trio, Siemens Healthcare, Erlangen, Germany), equipped with a whole-body gradient (40 mT/m, 200 T/m/s) and a 32-channel head coil. To minimize specific absorption rate (SAR) and noise exposure, we used radio-frequency impulsions with "no SAR," and "whisper" gradient mode.

A diffusion-weighted (DW) spin-echo single-shot echo-planar imaging (EPI) sequence was used, with parallel imaging (GRAPPA reduction factor 2), partial Fourier sampling (factor 6/8), and monopolar gradients to minimize mechanical and acoustic vibrations. After the acquisition of the $b = 0$ volume, diffusion gradients were applied along 30 orientations with $b = 700$ s mm^{-2}. Note that typically a b-value of 1000 s mm^{-2} is acquired for the adult brain. Images were here acquired with a smaller b-value to achieve a better signal-to-noise ratio while taking into account the higher diffusivity values related to the higher water content in the infant brain (Xing et al. 1997; Dubois et al. 2006). In infants, 50 interleaved axial slices covering the whole brain were acquired with a 1.8-mm isotropic spatial resolution [field of view = 230 × 230 mm^2, matrix = 128 × 128, slice thickness = 1.8 mm, echo time (TE) = 72 ms, and repetition time (TR) = 10 s], leading to a total acquisition time of 5 min 40 s which was reasonably short for unsedated infants. To enable quantitative comparisons of DTI parameters, the same protocol was used in adults, except that 70 slices were acquired to cover the whole brain (TR = 14 s to maintain a 200-ms acquisition time per slice).

For anatomical registration, T_2-weighted (T2w) images were acquired in infants using a 2D turbo spin-echo sequence (spatial resolution = 1 × 1 × 1.1 mm^3), and T_1-weighted (T1w) images were acquired in adults using a 3D fast gradient inversion recovery sequence (magnetization-prepared rapid gradient-echo sequence, 1 mm isotropic spatial resolution). In infants, T_2 weighting actually provides a better gray/white matter contrast than T_1 weighting (Dubois, Dehaene-Lambertz, et al. 2014).

Data Postprocessing and Bundle Tractography

Data Preparation and Postprocessing

All data were processed using the PTK toolkit and the Connectomist software both developed in-house at NeuroSpin (Duclap et al. 2012). DW images were first corrected for motion artifacts using a dedicated strategy (Dubois, Kulikova, et al. 2014), based on 2 successive steps: (1) Automated detection and 2D resampling of slices corrupted by motion or technical problems (e.g., mechanical vibrations and spike noise) and (2) 3D realignment of the 30-orientation volumes misregistered due to intervolume motion and distortions stemming from eddy current. During this procedure, all images were resampled to ensure proper co-registration with anatomical images and to align the anterior and posterior commissures in an axial plane. The DTI model was estimated in each voxel within a brain mask, and DTI maps [fractional anisotropy (FA), mean $\langle D \rangle$, longitudinal $\lambda_{//}$, and transverse $\lambda_{\perp}$ diffusivities] were generated.

To resolve the problem of crossing fibers, the bundles reconstruction was based on an analytical Q-ball model (Descoteaux et al. 2007) and on a tractography algorithm with regularization (Perrin et al. 2005). Using 30 diffusion orientations and a 700-s mm^{-2} b-value, a 4-order analytical Q-ball model was computed. Whole-brain 3D tractography was performed using regularized particle trajectories (Perrin et al. 2005) with an aperture angle of 45°. Each particle follows locally the direction of the strongest diffusion, except in voxels with low anisotropy due to fiber crossing, where the particle inertia favors a low curvature of the trajectory. Similar to diffusion tensor deflection (Lazar et al. 2003), this strategy resolves simple crossing configurations (Perrin et al. 2005) and is particularly adapted to reconstruct the infants' immature bundles despite their low myelination and anisotropy (Dubois, Dehaene-Lambertz, Perrin, et al. 2008). The seed mask within the white matter excluded voxels with either low FA (<0.15 for infants and <0.20 for adults) or high $\langle D \rangle$ (>2 × 10^{-3} mm^2 s^{-1}; Dubois et al. 2006; Dubois, Dehaene-Lambertz, Perrin, et al. 2008), which may correspond to gray matter and cerebro-spinal fluid (CSF). To get the cortical terminations of fibers, the tractography propagation was loosened to voxels with lower FA (FA >0.10 for infants and >0.15 for adults).

Identification of the Bundles of Interest

For all subjects, we identified the main bundles of the language network reported in adults (Catani and Thiebaut de Schotten 2008; Thiebaut de Schotten, Ffytche, et al. 2011). In the dorsal pathway, we dissected the AF and SLF, and in the ventral pathway the MLF, the ILF, and its lateral branches (ILFlat), the UF, iFOF and EC.

To retrieve these fascicles from the whole-brain tractography, we defined regions of interest (ROIs) that the tracts should cross (Catani et al. 2002; Huang et al. 2004) and regions of exclusion (ROEs), that is, "forbidden passages," where fibers should not pass (ROEs were necessary to avoid errors in regions of crossing

bundles). ROIs and ROEs were delineated in the native space of each participant, using reproducible landmarks across subjects (see Fig. 1 and Table 1 for the description of ROIs and ROEs). This was done on 2D slices from both the color-encoded directionality DTI map and the co-registered anatomical images, perpendicularly to the expected fibers using the Anatomist software (Riviere et al. 2000; http://brainvisa.info).

The EC fasciculus is a narrow tract, separated from the external capsule by the claustrum. Because its role in the developing language network has been emphasized in neonates (Perani et al. 2011), we tried to reconstruct it and to distinguish it from the iFOF (Turken and Dronkers 2011; Forkel et al. 2014). However, the claustrum separation was not visible on DW images because it was smaller than the voxel size. Because this bundle is supposed to connect the superior temporal gyrus and the inferior frontal lobe at the level of the pars triangularis (Brodmann area 45), we drew coronal ROIs at the level of extreme/external capsules and of Heschl's gyrus, and a large 3D ROI including the pars triangularis and opercularis (Fig. 1) to select this bundle.

Individual Measures of DTI Parameters

For each bundle, DTI parameters were quantified over the entire tract while taking the fiber density into account: line integration was used for each fiber of the tract by interpolating the DTI maps in 3D, and a mean value over the tract was computed by averaging the measurements from all points of all fibers (Dubois et al. 2006). We took advantage of the different sensitivities of DTI parameters (FA, longitudinal $\lambda_{//}$, and transverse $\lambda_{\perp}$ diffusivities) in relation with the tracts macro- and microstructural properties (Dubois, Dehaene-Lambertz, Perrin, et al. 2008; Dubois, Dehaene-Lambertz, et al. 2014), to study them alone and in combination.

Even in the absence of myelin, the tight organization of fibers inside a bundle (with high coherence, compactness, and density) creates intrinsic anisotropy due to high longitudinal diffusivity and low transverse diffusivity (Beaulieu 2002), whereas regions of crossing fibers display low anisotropy. Even if myelination has a strong impact on DTI parameters, each bundle may present a specific profile of parameters that remains constant across life, according to its geometry, compactness, composition in fibers, and its relations to neighboring structures (crossings, etc.). Maturation also strongly impacts DTI parameters. During the "pre-myelination" stage, decreases in both diffusivities are observed as the brain water content decreases and the density of hindering membranes increases (Dubois, Dehaene-Lambertz, Perrin, et al. 2008), and this process should already be anisotropic in favor of the axonal direction (Zanin et al. 2011; Nossin-Manor et al. 2013). Second, the "true" myelination stage (which consists of the ensheathment of axons by oligodendroglial processes) is accompanied by an increase in anisotropy and a decrease in transverse diffusivity (but no change in longitudinal diffusivity) as well as a decrease in membrane permeability and extracellular distance.

In regions of crossing fibers, the profile of DTI parameters may appear more complex, particularly when crossing bundles are maturing over different time periods (Dubois, Dehaene-Lambertz, et al. 2014). Let's compare a voxel 1 containing only bundle A, and a neighbor voxel 2 including bundle A (same density) and a crossing bundle B. These additional fibers in voxel 2 increase the global density, and thus mean and longitudinal diffusivities are lower in 2 than 1 ($\langle D\rangle_2 < \langle D\rangle_1$; $\lambda_{//2} < \lambda_{//1}$), and transverse diffusivity is higher ($\lambda_{\perp 2} > \lambda_{\perp 1}$). Nevertheless, simulations show that the relative difference between voxels 1 and 2 is lower for $\lambda_{\perp}$ than for $\lambda_{//}$: $|\lambda_{\perp 2} - \lambda_{\perp 1}|/\lambda_{\perp 1} < |\lambda_{//2} - \lambda_{//1}|/\lambda_{//1}$. If myelination starts earlier in bundle A than in bundle B, anisotropy

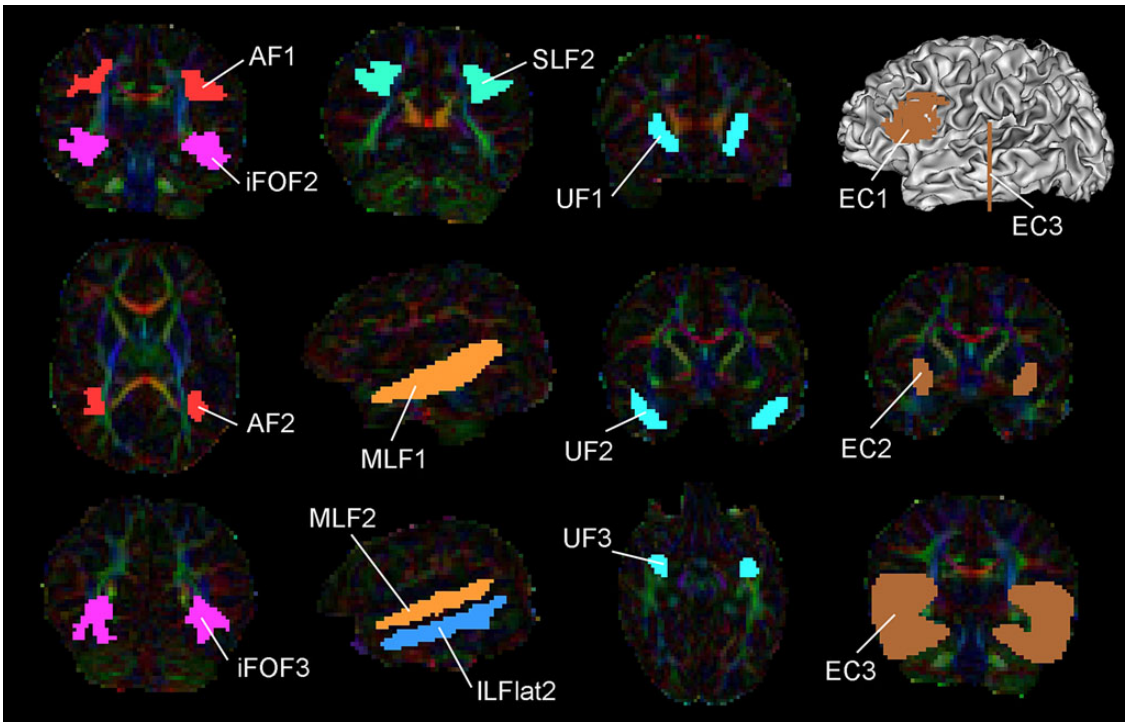

Figure 1. Selection of the bundles. ROIs used to select the bundles (Catani et al. 2002; Huang et al. 2004) are projected on the color-encoded directionality map for an infant (female, age 10 weeks old). The ROIs numbering corresponds to Table 1. AF: arcuate fasciculus; EC: extreme capsule; iFOF: inferior fronto-occipital fasciculus; ILF: inferior longitudinal fasciculus; ILFlat: lateral branches of the inferior longitudinal fasciculus; MLF: middle longitudinal fasciculus; SLF: superior longitudinal fasciculus; UF: uncinate fasciculus.

Table 1 Localization of ROIs and ROEs used for bundles dissection

Bundle	ROIs	ROEs
AF	(1) A parietal ROI: in the bundle upper parietal part, at the level of the posterior commissure on a coronal plane (2) A ROI at the parieto-temporal junction: at the level of the arcuate loop on an axial plane	(3) A core ROE including the internal and external capsules
SLF	(1) The AF parietal ROI (2) A parietal ROI more anteriorly: at the level of the splenium of corpus callosum on a coronal plane	(3) The AF loop ROI
UF	(1) A frontal ROI: at the level of the genu of corpus callosum on a coronal plane (2) A temporal ROI: at the level of the optic chiasm on a coronal plane (3) An intermediate ROI at the fronto-temporal junction: at the level of the bundle loop on an axial plane	
iFOF	(1) The UF frontal ROI (2) A temporal ROI: at the level of the posterior commissure on a coronal plane (3) An occipital ROI: at one third of the distance between the lateral geniculate nucleus and the occipital pole on a coronal plane	
ILF	(1) The UF temporal ROI (2) The iFOF temporal ROI (3) The iFOF occipital ROI	
MLF	(1) A large medial ROI: close to the AF and ILF trajectories on a sagittal plane (2) A lateral region: above the superior temporal sulcus on a sagittal plane	
ILFlat	(1) The MLF medial ROI (2) A lateral region: below the superior temporal sulcus on a sagittal plane	
EC	(1) A ROI including the pars opercularis and pars triangularis: using as borders the inferior pre-central sulcus, the inferior frontal sulcus, the infero-anterior frontal sulcus, and the insula based on the 3D reconstruction of the inner cortical surface (2) A ROI including the extreme and external capsules: at the level of the anterior commissure on a coronal plane (3) A temporal ROI: at the level of Heschl's gyrus on a coronal plane	(4) A parietal ROE: above the temporal ROI on a coronal plane

Note: To extract each bundle of the language network from the whole-brain tractography, we defined 2 or 3 ROIs and 0 or 1 ROEs for each infant and adult, according to reproducible anatomical landmarks. For abbreviations, see Figure 1.

increases in voxel 1 as soon as A gets myelinated, whereas transverse diffusivity (and longitudinal diffusivity but to a lower extent) decreases (Dubois, Dehaene-Lambertz, Perrin et al. 2008). In voxel 2, anisotropy first increases when A gets myelinated, then decreases when B starts myelinating, whereas transverse diffusivity keeps decreasing, as well as longitudinal diffusivity (but again to a lower extent). Thus, FA changes may be ambiguous and not related to similar phenomena in voxels 1 and 2, whereas myelination only decreases $\lambda\perp$ values (and $\lambda/\!/$ values to a lesser extent) in both voxels.

In summary, transverse diffusivity strongly decreases with all processes of white matter maturation, and thus this parameter is likely the best DTI marker of myelination (Song et al. 2002, 2005; Dubois, Dehaene-Lambertz, Soares, et al. 2008). On the contrary, FA and longitudinal diffusivity are good markers of tissue macrostructure and organization that finely characterize the bundle's coherence and compactness, but their changes with varying maturation may be more difficult to interpret particularly in regions of crossing fibers where tracts at different maturational stages may intermingle. Thus, we quantified and jointly analyzed the 3 parameters, that is, FA, $\lambda/\!/$, and $\lambda\perp$, to characterize the bundles macro- and microstructure, but focused on $\lambda\perp$ evolution to highlight maturational patterns across bundles.

Statistical Analyses

All analyses were first performed on DTI parameters (FA, $\lambda/\!/$, and $\lambda\perp$) to compare infants with adults and identify similarities and differences in the microstructure and organization of the language networks in both groups. In particular, we studied whether the same relationships across the bundle parameters remained at both ages, emphasizing their structural similarities.

Second, we investigated the asynchrony of maturation across bundles in the infant brain, by eliminating differences in geometry, compactness, and macro- and microscopic organization (Dubois, Dehaene-Lambertz, et al. 2014; Kulikova et al. 2014): infants' parameters were then normalized by the adult reference, that is, divided by the corresponding median over the adult group (Dubois, Dehaene-Lambertz, Perrin, et al. 2008; Dubois, Dehaene-Lambertz, Soares, et al. 2008). These normalized parameters were noted as nFA, n$\lambda/\!/$, and n$\lambda\perp$.

Bundle Clustering

Because previous studies insisted on the role of the EC during the first post-natal months (Perani et al. 2011; Brauer et al. 2013), we first investigated whether this bundle was distinguishable from the iFOF, independently in the infant and adult groups. Analyses of variance (ANOVAs) were performed to highlight the effects of bundles on each DTI parameter (FA, $\lambda/\!/$, and $\lambda\perp$), and Tukey analyses were used to evaluate differences between pairs of bundles while taking into account multiple comparisons.

Second, we performed hierarchical clustering of the bundles to explore whether pathways of the language network may be grouped into classes according to common microstructural properties. Clustering was based on the 3 DTI parameters, using Euclidian distances and an average linkage approach implemented in Python with NumPy (www.numpy.org) and StatsModels (Seabold and Perktold 2010). The basic concept of this approach was to build a hierarchy of classes based on a measure of dissimilarity between bundles. For each pair of bundles, the Euclidian distance was computed from DTI parameters quantified in the 2 bundles, and a matrix of all pairwise distances was generated. The

hierarchical clustering was initialized by grouping the bundles with minimal distance, and the procedure was repeated iteratively. To compare groups of bundles with each other, the average linkage criterion was used. The resulting tree diagram ("dendrogram") illustrated the arrangement of bundles in classes, and the heights of its branches were proportional to the dissimilarities between the bundles. This approach of hierarchical clustering was undertaken on 2 distinct datasets: (1) on DTI parameters in the adult group (jointly for FA, $\lambda_{//}$, and $\lambda_{\perp}$) to examine bundle similarities in microstructural properties and (2) on normalized DTI parameters in the infant group (first jointly for nFA, $n\lambda_{//}$, and $n\lambda_{\perp}$; second only for $n\lambda_{\perp}$ which appeared the most pertinent parameter of maturation) to consider bundle similarities in maturational properties. For each DTI parameter and subject, the classes identified by the hierarchical clustering were characterized by the averages computed over corresponding bundles. To determine which parameter mostly influenced the classes discrimination from these 2 exploratory analyses, paired Student's *t*-tests were then performed between classes over the group of interest (*t*-values are reported, but not *P*-values to avoid circular argument among inference, where the classes identification with hierarchical clustering and the classes comparison were performed on the same data). Besides, classes identified through the clustering in the adult group were compared in the infant group for each DTI parameter using ANOVA with Tukey analyses.

Bundle Asymmetries

Because of the known left-right asymmetries in the organization and maturation of the language network (Dubois, Benders, et al. 2008; Dubois et al. 2009, 2010; Glasel et al. 2011; Leroy et al. 2011), we computed an asymmetry index (AI) for each DTI parameter, *P* (normalized or not), in each bundle: $AI = (P(L) - P(R))/(P(L) + P(R))$, where L and R denote the left and right sides, respectively. The significance of nonzero asymmetry indices was independently tested over the infant and adult groups using one-sample Student's *t*-test (two-tailed) with a significance level of $P_{adj} < 0.05$ after correction for multiple comparisons with a false discovery rate (FDR) approach (additionally trends up to $P_{adj} < 0.10$ were reported if $P < 0.05$).

Maturational Changes

Because transverse diffusivity $\lambda_{\perp}$ is thought to be the best DTI marker of myelination, we focused on its normalized value to further investigate maturational relationships across the bundles. We assessed whether dorsal and ventral bundles displayed different patterns of maturation over this short developmental period. Conversely, the age-related variation of $n\lambda_{\perp}$ was evaluated in each bundle via linear regressions, and the slopes were correlated across all bundles with the parameter medians over the infant group (significant results: $P_{adj} < 0.05$, trends: $P_{adj} < 0.10$). We also evaluated the age-related changes in the classes resulting from hierarchical clustering by computing the $n\lambda_{\perp}$ averages over the bundles within each of the classes; we further investigated whether these classes displayed converging, diverging, or parallel patterns of maturation compared with the average over all bundles.

Results

Common Organization of the Language Pathways in Infant and Adult Brains

Visual Inspection of the Tractography

Despite their weak maturation, all bundles were reconstructed in each infant and showed trajectories similar to those of adults (Fig. 2). The AF was the most variable bundle; specifically, the infants' fronto-parietal segment was either limited to the precentral region, terminated more posteriorly in the parietal lobe (behind the central sulcus), or extended to the frontal lobe. In the temporal lobe, the fiber projections of the AF wrapped up the STS to terminate in the superior and middle temporal gyri. This sulcus was also surrounded by, above, short fibers from the MLF and below, the lateral branches of the ILF. Regarding the ventral fronto-temporal connections, the EC was difficult to distinguish from the iFOF in infants and adults, particularly at the level of the extreme/external capsules and in the temporal lobe. The EC frontal projections were more lateral than the iFOF, including in the pars opercularis and triangularis, because of the ROI definition.

Analyses of DTI Parameters

The averaged DTI parameters were quantified over the whole tracts to minimize the potential interindividual variability in tract reconstruction. Although the DTI parameters significantly differed between infants and adults (with, as expected, lower anisotropy and higher diffusivities in infants than in adults), the median values of both groups strongly correlated across bundles for FA (correlation coefficient $r = 0.93$, $P < 0.001$; Fig. 3*a*) and $\lambda_{//}$ ($r = 0.87$, $P = 0.005$; Fig. 3*b*), whereas the trend for $\lambda_{\perp}$ was not significant ($r = 0.49$; Fig. 3*c*). All DTI parameters depend both on the arrangement of fibers within the bundle and on myelination. Nevertheless, $\lambda_{\perp}$ is more strongly affected by all stages of maturation than FA and $\lambda_{//}$, and is weakly affected by crossing fibers (see the Materials and Methods section), making it a better marker of myelination. We thus interpreted this lower correlation for $\lambda_{\perp}$ as the result of its best sensitivity to different maturation stages across bundles, which may have masked the structural similarities between infants and adults.

The ANOVAs confirmed a strong bundle effect for each DTI parameter and both ages (infants/adults: FA—$F = 70.4/56.7$; $\lambda_{//}$—$F = 22.2/81.7$; $\lambda_{\perp}$—$F = 9.1/21.1$; $P < 0.001$), but Tukey tests did not distinguish the iFOF and the EC for any parameter and any group except for the longitudinal diffusivity in the adult group ($P < 0.001$). This finding suggests that, in addition to their close trajectories, the microstructures of these 2 bundles were similar (thus, the iFOF and EC were considered together in all analyses except in the hierarchical clustering over adults).

In the adult group, the hierarchical clustering of the bundles based on FA, $\lambda_{//}$, and $\lambda_{\perp}$ (Fig. 3*d*) demonstrated 3 classes with a strong segregation between (1) short-distance fibers (MLF and ILFlat branches), (2) dorsal pathways (AF and SLF), and (3) ventral pathways (UF, EC, iFOF and ILF). The averages over all bundles of each class were also considered for each DTI parameter, and paired Student's *t*-tests between classes (Fig. 3*e*) highlighted that all 3 parameters provided relevant information for the classes discrimination (Fig. 3*a*–*c*,*e*: the ventral class displayed mainly higher $\lambda_{//}$ than the 2 other classes, and the dorsal class displayed mainly higher FA and lower $\lambda_{\perp}$ than the short fiber class).

We secondly tested whether the same 3 classes of bundles were pertinent for infants. Paired Student's *t*-tests for each DTI parameter (Fig. 3*e*) highlighted that these classes strongly differed in terms of FA (Fig. 3*a*–*c*,*e*), as confirmed by ANOVAs for effects of classes (FA—$F = 108.5$, $P < 0.001$; $\lambda_{//}$—$F = 17.5$, $P < 0.001$; $\lambda_{\perp}$—$F = 7.7$, $P = 0.001$). According to Tukey tests (Fig. 3*e*), the short fibers and ventral pathways significantly differed, but the distinction between the dorsal pathways and the 2 other classes was not significant in terms of $\lambda_{\perp}$.

These results suggested commonalities in the microstructures of infant and adult bundles that are concurrent with

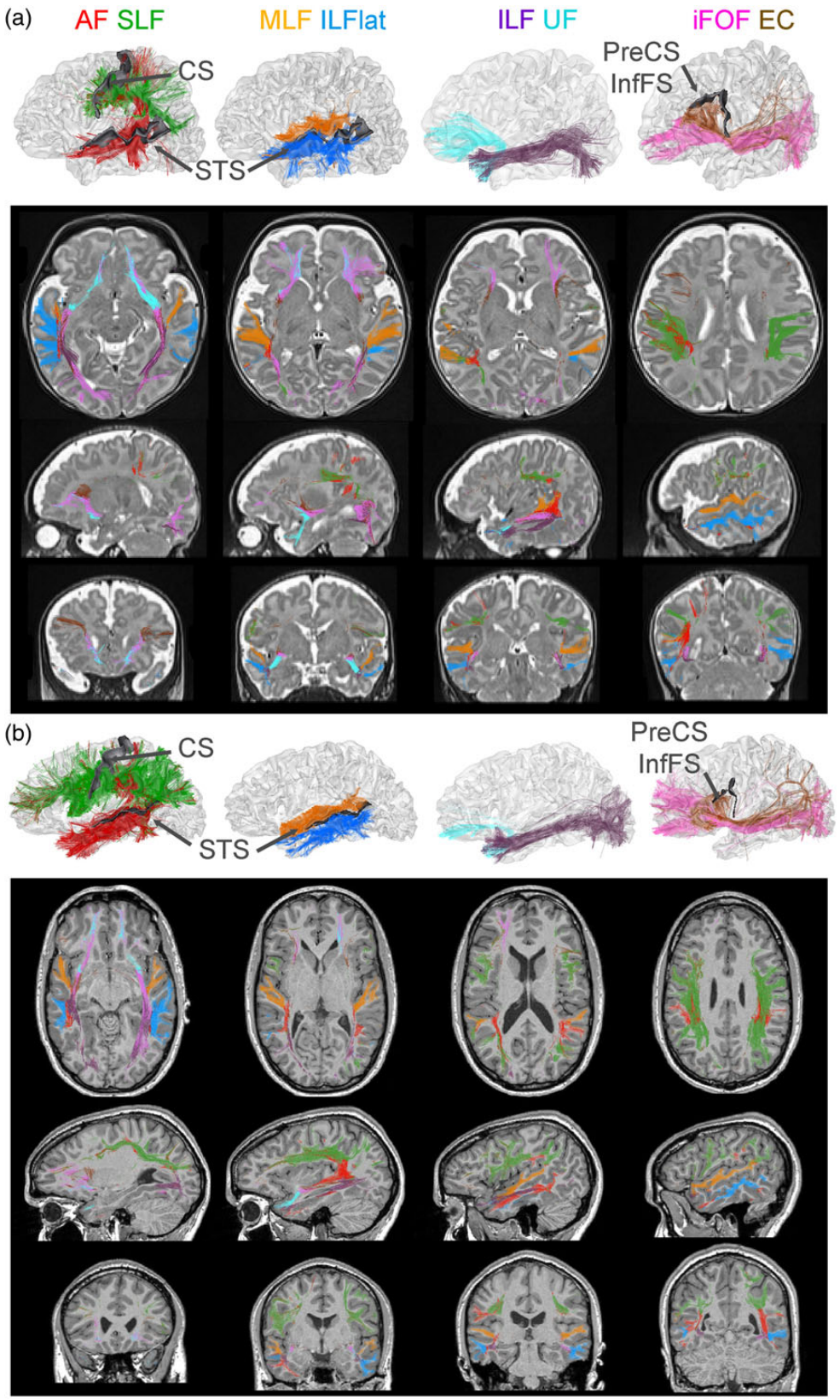

Figure 2. Individual trajectories of linguistic bundles. The reconstructions by tractography of the white matter bundles involved in the language network are presented for a single infant (*a*: male, age 7 weeks old) and a single adult (*b*: male, age 22.5 years old). On the upper row, tracts of the left hemisphere are superimposed on the 3D reconstruction of the inner cortical surface, and particular sulci are highlighted in gray (the superior temporal sulcus, the central sulcus, and sulci bordering Broca's region on the left side: the pre-central sulcus and the inferior frontal sulcus). On the 3 lower rows, tracts are superimposed on anatomical images (*a*: T2w for the infant and *b*: T1w for the adult, which provide the best contrast between gray and white matter, respectively) presented on axial, sagittal (left side), and coronal views at equivalent positions for the 2 subjects. For abbreviations, see Figure 1; CS: central sulcus; InfFS: inferior frontal sulcus; PreCS: pre-central sulcus; STS: superior temporal sulcus.

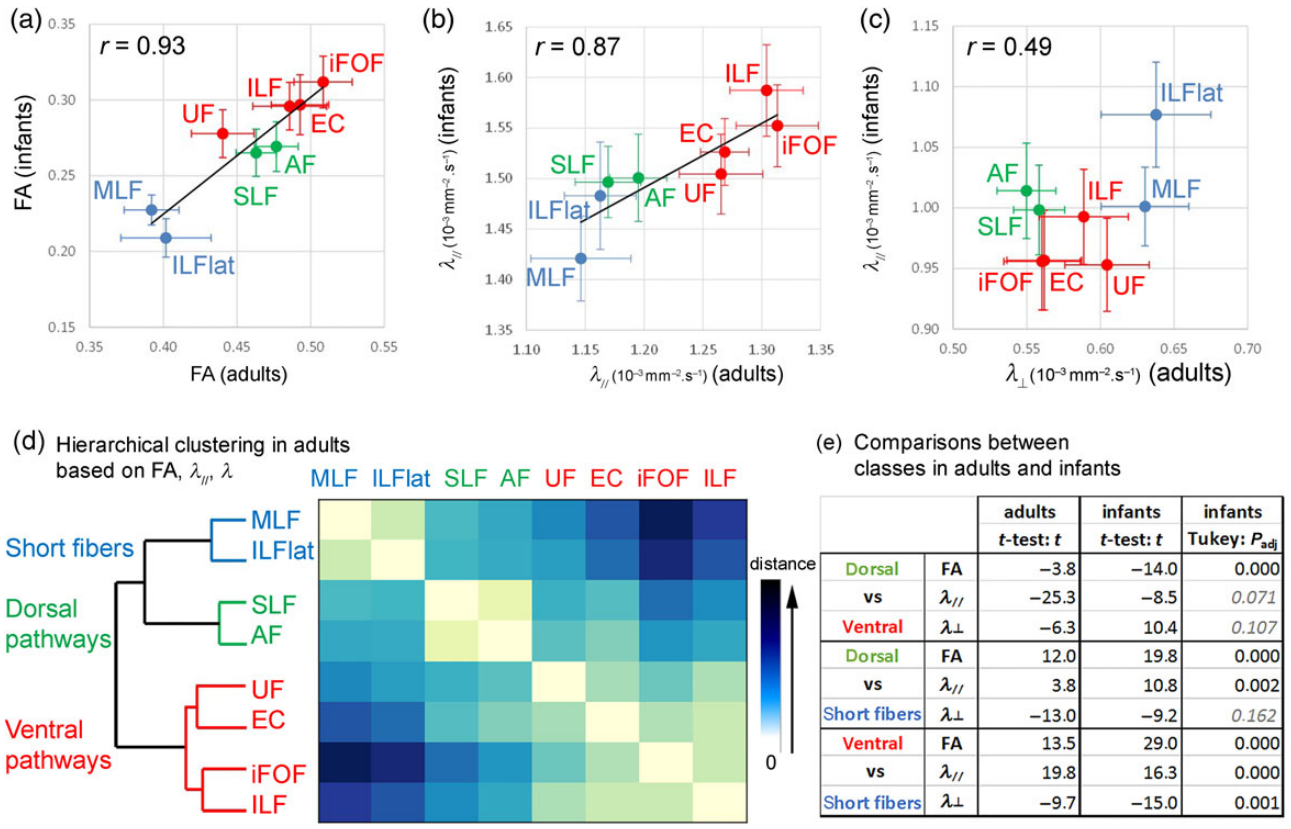

		adults t-test: t	infants t-test: t	infants Tukey: P_{adj}
Dorsal	FA	−3.8	−14.0	0.000
vs	$\lambda_{//}$	−25.3	−8.5	*0.071*
Ventral	$\lambda_{\perp}$	−6.3	10.4	*0.107*
Dorsal	FA	12.0	19.8	0.000
vs	$\lambda_{//}$	3.8	10.8	0.002
Short fibers	$\lambda_{\perp}$	−13.0	−9.2	*0.162*
Ventral	FA	13.5	29.0	0.000
vs	$\lambda_{//}$	19.8	16.3	0.000
Short fibers	$\lambda_{\perp}$	−9.7	−15.0	0.001

Figure 3. Comparing the microstructure of linguistic bundles in infants and adults. (*a*–*c*) DTI parameters (*a*: anisotropy; *b*: longitudinal diffusivity; *c*: transverse diffusivity) were quantified in the bundles over the groups of infants and adults (median values are presented; error bars show standard deviations over each group, computed after removing age effects in infants; colors correspond to the clustering presented in *d*). They demonstrated large differences across bundles and across groups (with smaller anisotropy and higher diffusivities in infants), together with correlations between infants and adults (correlation coefficients *r* were calculated over all bundles). (*d*) The hierarchical clustering was computed from FA, $\lambda_{//}$, and $\lambda_{\perp}$ in the adult group: short fibers (in blue), dorsal pathways (in green), and ventral pathways (in red) were distinguished on the dendrogram, which was computed from Euclidian distances (coded in blue scale on the matrix of pairwise distances across bundles) and average linkage criterion. (*e*) Differences between pairs of classes in each DTI parameter were further investigated using paired Student's *t*-tests in both the adult and infant groups (*t*-values are reported) and Tukey analyses associated with ANOVAs in the infant group (adjusted *P*-values are reported; italic gray font corresponds to $P_{adj} > 0.05$). For abbreviations, see Figure 1.

maturational differences, which primarily impact the transverse diffusivity ($\lambda_{\perp}$).

Asymmetries in Microstructure and Organization

Anisotropy in the AF was strongly asymmetric toward the left side in infants ($t = 5.1$, $P_{adj} = 0.001$) and adults ($t = 4$, $P_{adj} = 0.017$), which agrees with previous studies (Buchel et al. 2004; Dubois et al. 2009; Liu et al. 2010). In the adult group, the transverse diffusivity of this fasciculus also tended to be asymmetric ($t = -2.8$, $P_{adj} = 0.094$). The number of reconstructed fibers was asymmetric toward the left side in the adult AF ($t = 4.1$, $P_{adj} = 0.017$) and toward the right side in the iFOF-EC bundle ($t = -3.8$, $P_{adj} = 0.017$), which agrees with a previous atlas-based study (Thiebaut de Schotten, Ffytche, et al. 2011). Asymmetry was not observed for any other infant bundle, while leftward asymmetries were detected for the longitudinal diffusivity in the adult UF ($t = 3.3$, $P_{adj} = 0.043$) with a trend in the ILF ($t = 2.7$, $P_{adj} = 0.094$).

In summary, these analyses based on tractography and DTI parameters demonstrated several similarities between infants and adults: (1) the overall architecture and trajectory of pathways, (2) the microstructural segregation between short fibers, ventral, and dorsal pathways (except in terms of $\lambda_{\perp}$, because this parameter crucially reflects the bundle maturation in infants), and (3) the strong asymmetry in the anisotropy of the AF, which indicates a higher fiber density and greater bundle compactness and/or fewer crossing fibers in the left hemisphere.

Asynchronous Maturation of Dorsal and Ventral Pathways

In addition to the intrinsic bundle properties that strongly affect DTI parameters, differences detected among bundles in the infant group might relate to distinct maturational tempos. Thus, we also studied the data from infants normalized by the data from adults in order to disentangle between maturational differences across bundles and differences in the tracts geometrical characteristics (e.g., shape and compactness).

Asymmetries in Maturation

The analysis of normalized DTI parameters highlighted several differences between the left and right hemispheres in the infant group (Fig. 4). In the AF, a trend toward a higher left nFA ($t = 2.5$, $P_{adj} = 0.057$) associated with a higher $n\lambda_{//}$ ($t = 2.6$, $P_{adj} = 0.052$) suggested maturational asymmetries in the fiber coherence, bundle compactness, or amount of crossing fibers. Similarly, the SLF was asymmetric toward the left side in infants, with a higher fiber coherence reflected by a higher $n\lambda_{//}$ ($t = 3.4$, $P_{adj} = 0.015$) combined with a higher nFA ($t = 2.4$, $P_{adj} = 0.058$) and lower $n\lambda_{\perp}$ ($t = -2.6$, $P_{adj} = 0.052$). Like in the MLF, the nFA was higher in the left

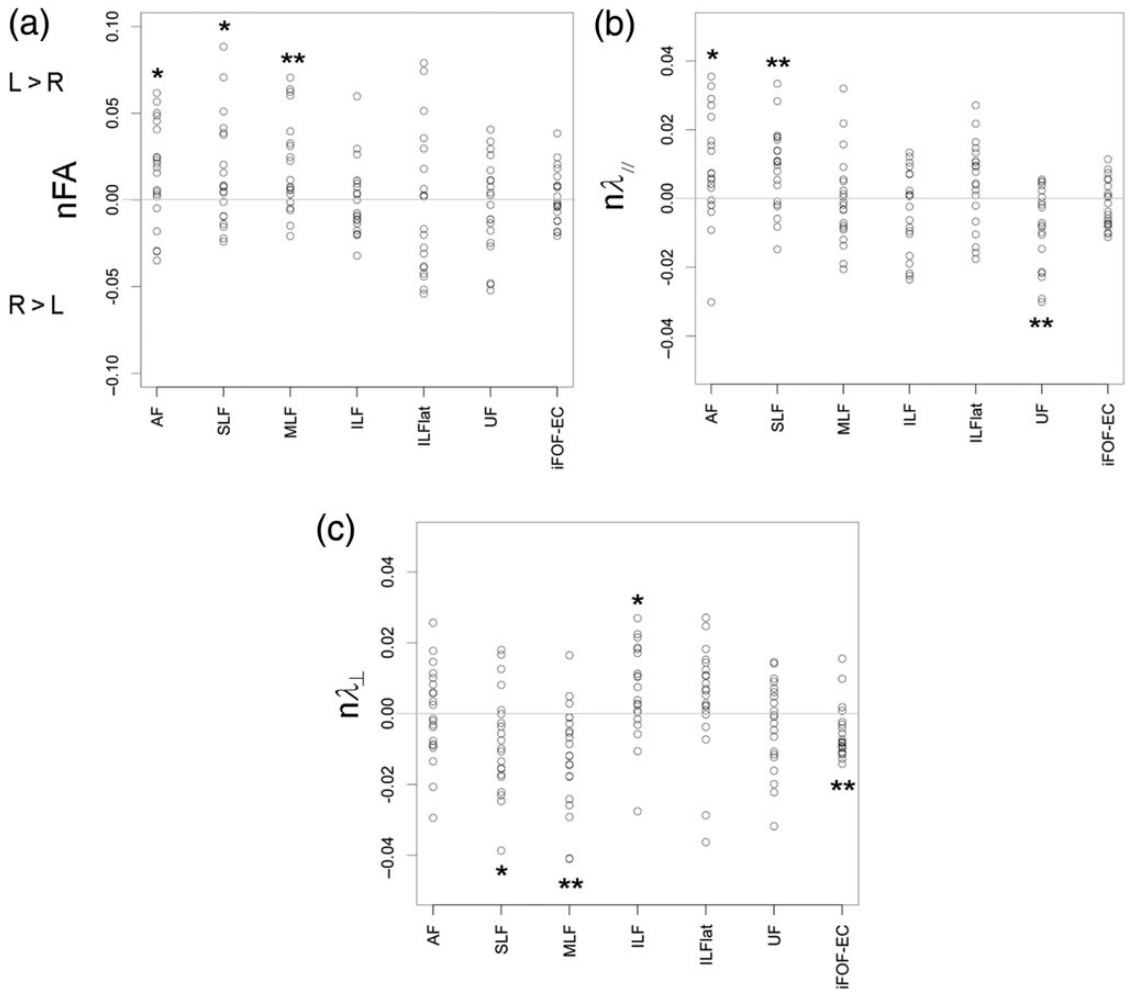

Figure 4. Asymmetries in maturation of linguistic bundles. Asymmetry indices between the left and right hemispheres AI = $(P(L) - P(R))/(P(L) + P(R))$ are presented for normalized FA (*a*), longitudinal (*b*), and transverse (*c*) diffusivities for all infants of the group. Statistically significant asymmetries are outlined [one-Student's *t*-test with *P*-threshold adjusted for multiple comparisons (FDR): $^{**}P_{cor} < 0.05$; $^{*}P_{cor} < 0.06$]. For abbreviations, see Figure 1.

hemisphere ($t = 3.2$, $P_{adj} = 0.019$) in relation with lower $n\lambda\perp$ ($t = -3.9$, $P_{adj} = 0.015$), suggesting either again a higher fiber coherence or higher myelination. Other maturational asymmetries were detected in the ventral bundles (in the UF $n\lambda_{//}$: $t = -3.4$, $P_{adj} = 0.015$; in iFOF-EC $n\lambda\perp$: $t = -3.4$, $P_{adj} = 0.015$; in ILF $n\lambda\perp$: $t = 2.4$, $P_{adj} = 0.06$), but the underlying mechanisms could not be assessed because of the lack of conjunctions between the parameters. Despite these asymmetries were statistically significant, their amplitude was rather small: for all infants and bundles, asymmetry indices were lower than 10% for nFA and lower than 5% for $n\lambda_{//}$ and $n\lambda\perp$ (Fig. 4). Because of these maturational differences between hemispheres, the left and right bundles were independently considered in the following analyses.

Different Stages of Maturation

According to the clustering analysis of normalized DTI parameters (Fig. 5*a*–*c*), 3 maturation classes were identified in the bundles of the infant language network (Fig. 5*d*). The first class grouped all dorsal pathways (left and right AF and SLF), whereas the second and third classes included all ventral bundles (left and right iFOF-EC bundles, ILF and ILFlat branches on the one hand; left and right MLF and UF on the other hand). For all bundles, left and right tracts were clustered in the same classes, highlighting that differences in maturation between hemispheres (Fig. 4) were smaller than those across bundles (Fig. 5*a*–*c*). Note that interindividual variability further differed across bundles and hemispheres, probably because of different patterns of age-related changes.

The clustering computed only based on the normalized transverse diffusivity was very similar, and even better distinguished between classes (Fig. 5*e*). Based on the averages over each class for each normalized DTI parameter, paired Student's *t*-tests confirmed that $n\lambda\perp$ was more pertinent than nFA and $n\lambda_{//}$ for the class discrimination (Fig. 5*f*). Because this parameter is thought to be the best DTI marker of white matter maturation and should negatively correlate with age during the pre-myelination and "true myelination" of bundles (Dubois, Dehaene-Lambertz, Soares, et al. 2008; Dubois, Dehaene-Lambertz, et al. 2014), these results highlighted that the maturation of dorsal and ventral pathways strongly differed during this period of development: the $n\lambda\perp$ values of dorsal bundles were the highest (higher than the average over all bundles, Fig. 5*c*), suggesting that dorsal bundles are less mature than ventral bundles during the first post-natal weeks.

Different Patterns of Maturation

We further analyzed the patterns of maturation to investigate whether dorsal bundles continued to lag behind ventral bundles

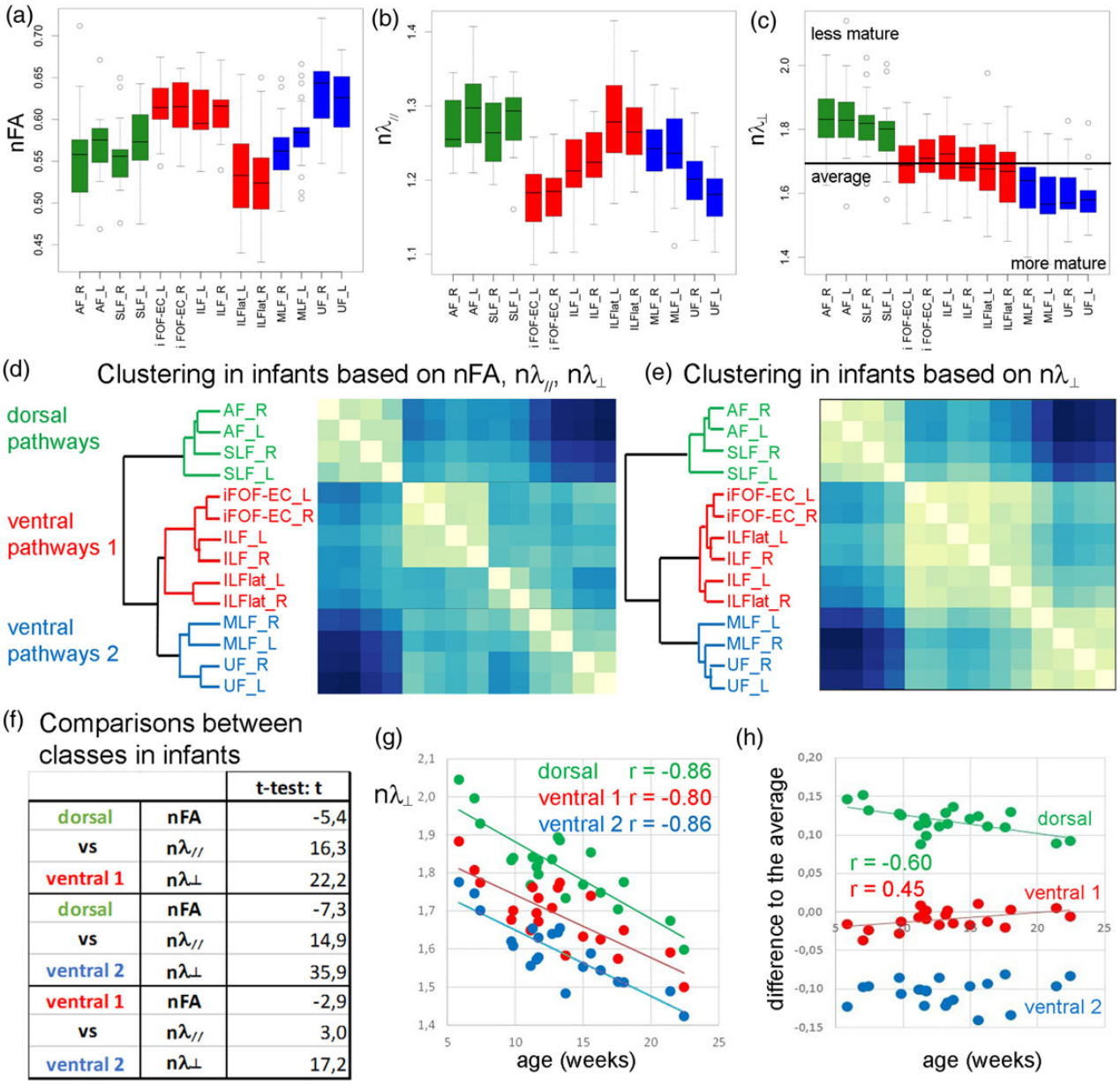

		t-test: t
dorsal	nFA	-5,4
vs	nλ//	16,3
ventral 1	nλ⊥	22,2
dorsal	nFA	-7,3
vs	nλ//	14,9
ventral 2	nλ⊥	35,9
ventral 1	nFA	-2,9
vs	nλ//	3,0
ventral 2	nλ⊥	17,2

Figure 5. Distinct maturation of the dorsal and ventral pathways. (*a*–*c*) Normalized DTI parameters (*a*: anisotropy; *b*: longitudinal diffusivity; *c*: transverse diffusivity) were quantified over the infant group (colors correspond to the clustering in *d*). (*d* and *e*) Hierarchical clustering separated the bundles into 3 main classes, whether the 3 parameters were considered (*d*) or only nλ⊥ (*e*), the most pertinent DTI parameter to study maturational differences. The 3 classes segregated: (1) dorsal pathways (in green: left and right AF and SLF), (2) part of the ventral pathways (in red: left and right iFOF-EC, ILF, and ILFlat), and (3) the other ventral pathways (in blue: left and right MLF and UF). Boxplots in nλ⊥ (*c*) demonstrated that bundles of these classes showed distinct maturational stages (the line indicates the average over all bundles): bundles with the highest nλ⊥ were the least mature, whereas bundles with the lowest nλ⊥ were the most mature. (*f*) Paired Student's *t*-tests, performed for each DTI parameter over the infant group, highlighted that differences between classes were important mainly in terms of nλ⊥ (*t*-values are reported). (*g* and *h*) The averages in nλ⊥ over each class strongly decreased with the increasing infants' age (*g*), and got closer to the average over all bundles (*h*: differences to the average got closer to 0). L: left; R: right; for abbreviations, see Figure 1.

or eliminated their delay during this developmental period. In the infant group, age-related decreases in nλ⊥ were observed in all left and right bundles ($r < -0.7$, $P_{adj} < 0.001$) and in the 3 classes of bundles (Fig. 5*g*: $r < -0.8$, $P_{adj} < 0.001$). The nλ⊥ slopes differed among bundles (e.g., near −0.021/week of age in the AF, near −0.015/week of age in iFOF-EC bundles), and the nλ⊥ slopes and nλ⊥ medians tended to correlate across all bundles ($r = 0.44$, $P = 0.094$), which suggested that the lower the maturation of a bundle was, the higher its maturational changes were. Specifically, the nλ⊥ average over each class approached the nλ⊥ average over all bundles as the age increased (Fig. 5*h*: dorsal class $r = -0.6$, $P_{adj} = 0.011$; first ventral class: $r = 0.45$, $P_{adj} = 0.057$; second ventral class: $r = 0.12$, not significant), suggesting that the maturation of all bundles homogenized over the 16-week period. The difference in maturation between the dorsal and ventral pathways significantly decreased with age (dorsal class vs. the first ventral class: $r = -0.61$, $P = 0.003$; dorsal class vs. the second ventral class: $r = -0.44$, $P = 0.048$). Thus, the maturation of dorsal pathways caught up the maturation of ventral pathways during the first post-natal weeks.

Discussion

In this cross-sectional diffusion imaging study of infants aged 6–22 weeks, we focused on the fronto-parieto-temporal connections within the language network at the very early period of language acquisition, when infants begin to vocalize. We reported 3 main results. First, we demonstrated that the linguistic pathways were similarly organized in infants and adults in terms of the macroscopic trajectory, asymmetry, and microstructure. In particular, we observed a segregation between the dorsal and ventral pathways at both ages, which has never been described so far. Second, we highlighted for the first time the different maturational calendars of these 2 systems of bundles: the dorsal bundles were less mature than the ventral bundles during infancy, but this gap closes over the first weeks of post-term life. Finally, at the methodological level, we proposed refined in vivo imaging approaches to reliably study the bundles microstructure and maturation, notably describing an original technique to cluster fascicles based on all 3 DTI parameters which takes benefit of their complementarity.

Early Organization of the Language Network

Dissecting Linguistic Bundles in the Infant Brain

In the developing brain as in the adult brain, a large-scale network of perisylvian regions, including the superior temporal, inferior parietal, and inferior frontal regions, is involved during speech processing (Dehaene-Lambertz et al. 2002; Dehaene-Lambertz, Hertz-Pannier, et al. 2006; Dehaene-Lambertz et al. 2010; Price 2010; Pallier et al. 2011; Mahmoudzadeh et al. 2013). The early combined activity of these remote cortical regions requires the long-distance fibers that connect the temporal, parietal, and frontal lobes to be minimally efficient starting during the last trimester of human pregnancy (Mahmoudzadeh et al. 2013). Two pathways circle the perisylvian regions and connect the inferior frontal and superior temporal regions. In the macaque brain, auditory information mainly flows ventrally and anteriorly, projecting toward the ventrolateral prefrontal cortex via the EC and participating in object identification and conspecific recognition (Petrides and Pandya 2009; Rauschecker and Scott 2009). In humans, the dorsal pathway is enlarged even when compared with that of chimpanzees, and this increase is due to the development of the AF (Rilling et al. 2008, 2012).

In this study, we observed similar trajectories for all linguistic bundles across infants and adults, which agree with the early growth of long associative connections during the preterm period (Huang et al. 2006; Vasung et al. 2010; Takahashi et al. 2012). Nevertheless, fiber pruning occurs throughout the first post-natal year (Rakic and Riley 1983; Kostovic and Rakic 1990; LaMantia and Rakic 1990, 1994; Petanjek et al. 2011; Kostovic et al. 2014), and one may have expected supplementary perisylvian connections to be observed in the infant brain relative to the adult brain. It was not the case in the present MRI study, suggesting that pruning is mostly completed during the first post-natal weeks, or that technical issues prevented their detection in vivo. In particular, due to the low myelination of the infant's tracts, the choice of ROIs was crucial to help the reconstruction algorithm. Because ROIs cannot be determined for unexpected connections, they cannot be actively looked for and only an improvement in data acquisition and analyses procedure will resolve this question. Here, to keep acquisition time short, the DWI protocol only included a limited number of diffusion orientations (30) with a relatively low b-value ($b = 700$ s mm^{-2}). This limitation in the number of diffusion orientations was similar to other studies at this age (Song et al. 2014). Relative to Song et al., we preferred a higher spatial resolution (1.8 mm isotropic resolution, i.e., 5.8 mm^3 volume, vs. 2 mm isotropic resolution, i.e., 8 mm^3 volume) to a higher diffusion weighting ($b = 700$ vs. 1000 s mm^{-2}). Although in adults a b-value of 1000 s mm^{-2} is typically acquired, the water content and thus the mean diffusivity values are higher in the infant brain. Thus, a smaller b-value in infants is reasonable according to the optimization method described by Xing et al. (1997) and Dubois et al. (2006). Whereas high angular resolution diffusion imaging (HARDI) in adults is generally based on a 6-order analytical Q-ball model (requiring the estimation of 28 coefficients; Descoteaux et al. 2007), we were able with our protocol to compute only a 4-order model (requiring the estimation of 15 harmonic coefficients). Nevertheless, this simpler Q-ball model combined with a regularization-based tractography algorithm (Perrin et al. 2005) allowed a stable reconstruction of the bundles across subjects, except in the regions of major crossroads.

The most important variability in bundle trajectory across subjects was the frontal ending of the AF. Its crossings with the corpus callosum and the cortico-spinal tract fanning along the central sulcus prevented the perfect delineation of its terminations. Because the cortico-spinal tract matures before associative bundles (Flechsig 1920; Brody et al. 1987; Kinney et al. 1988; Dubois, Dehaene-Lambertz, Perrin et al. 2008; Kulikova et al. 2014), transient local changes in anisotropy may arise during infancy in the low corona radiata that crosses the AF (Dubois, Dehaene-Lambertz, et al. 2014). As previously reported in newborns (Perani et al. 2011; Brauer et al. 2013), the AF often ended in infants in the premotor cortex rather than in the inferior frontal gyrus, like in adults. Contrarily to previous studies, we interpret this finding as a technical artifact and not as a pathway difference: the AF is bidirectional (with temporo-frontal and fronto-temporal fibers; Matsumoto et al. 2004; David et al. 2013); thus, fibers initiating from the inferior frontal region should have started to grow during the last weeks of pregnancy and should be observed in infants, if not during pregnancy. We suspect that the rapid maturation of the cortico-spinal tract prevents the accurate observation of the AF through crossings in the corona radiata. This problem may be more pronounced in DTI-based tractography (Perani et al. 2011; Brauer et al. 2013) compared with our approach, which is based on a Q-ball model and tractography with regularization. In the future, this crossing-fiber issue should be investigated using HARDI imaging, as facilitated by the advent of the multiband multi-slice EPI technique (Feinberg et al. 2010; Moeller et al. 2010), which drastically decreases the acquisition time and thus enables to increase the number of diffusion orientations and thus the b-value in spontaneously asleep healthy infants.

In recent years, studies have suggested that the EC is a major linguistic pathway in adults (Frey et al. 2008; Saur et al. 2008; Makris and Pandya 2009; Wong et al. 2011), children (Brauer et al. 2011), and neonates (Perani et al. 2011). Given the small size of this structure, our study lacked the spatial resolution to avoid partial volume effects with the external capsule, a problem also present in previous studies in newborns (Brauer et al. 2013) and adults (Catani and Mesulam 2008; Martino et al. 2010; Turken and Dronkers 2011; Forkel et al. 2014). The 2 walls of gray matter that delimit the EC (insula and claustrum) were less distant than the voxel size, making the trajectory and microstructure of iFOF and EC very similar in both the infant and adult groups. We thus considered these 2 bundles together as a ventral pathway in the maturational analyses. To date, only postmortem studies that use high spatial resolution tools can separate these bundles

in humans. Indeed, analysis of an adult brain with polarized light imaging recently highlighted that fibers from the iFOF were visible in the ventral part of both the external capsule and EC (Axer et al. 2012).

Early Differences in the Microstructure of Dorsal and Ventral Pathways

We also investigated whether linguistic bundles may be grouped in distinct classes with a hierarchical clustering based on DTI parameters in the adult group. FA as well as longitudinal and transverse diffusivities were jointly used, because these quantitative parameters provide complementary information on bundle microstructure (Dubois, Dehaene-Lambertz, et al. 2014). As in adults, a clear distinction was observed between the dorsal pathway (AF and SLF) and the ventral pathway (EC, iFOF, and UF) in infants, suggesting a stable and consistent organization of the language network in terms of connectivity and microstructure (e.g., coherence, compactness, and density). Beyond the maturational processes that occur in these pathways (see Discussion below), their early organization in the infant brain may be the anatomical substrate that enables temporal and frontal regions to efficiently communicate and process speech.

Language Lateralization and Interhemispheric Asymmetries

Interhemispheric asymmetries were observed in both infants and adults. The main asymmetry concerned the AF, which displayed a higher left than right anisotropy. This asymmetry agrees with several previous studies (Buchel et al. 2004; Parker et al. 2005; Dubois et al. 2009; Liu et al. 2010). The left fasciculus was also larger than the right in adults, which is consistent with the findings of a previous study (Thiebaut de Schotten, Ffytche, et al. 2011). Nevertheless, the asymmetries in microstructure (FA) and macrostructure (number of fibers) did not correlate with each other. As suggested in children aged 7–11 years (Yeatman et al. 2011), the reconstruction of fewer fibers on the right side may be the result of a technical limitation in tracking a small fasciculus in a region with many crossing fibers rather than an extreme hemispheric dimorphism. Asymmetry in anisotropy might be a stronger marker of lateralization, although this relationship was not identified in a recent study (Song et al. 2014). This lack of asymmetry may have been due to the small sample size ($n = 12$) that covered a large age range (0–3 years), or the rougher spatial resolution in this study than the one utilized here (8 vs. 5.8 mm^3) that may have merged in the same voxels the AF and the SLF, which shows a reverse asymmetry in the adult brain (Thiebaut de Schotten, Dell'Acqua, et al. 2011). We observed other asymmetries that affected the ventral pathways (iFOF-EC, UF, and ILF) in the adult brain, and these findings partly replicated a previous study (Thiebaut de Schotten, Ffytche, et al. 2011).

The interhemispheric asymmetries within the language network found here are in agreement with the general assumption that the dorsal pathway is largely left-hemispheric dominant, while the ventral pathway is more bilaterally organized (Hickok and Poeppel 2007). This intrinsic asymmetry of the AF might be the white matter analog of the strong morphological asymmetries detected early on in perisylvian areas: Heschl's gyrus, planum temporale, and the anterior region of the Sylvian fissure (close to Broca's area) are commonly larger in the left hemisphere of the fetus and infant brain, whereas the superior temporal sulcus folds first and remains deeper in the right hemisphere (Witelson and Pallie 1973; Chi et al. 1977; Dubois, Benders, et al. 2008; Dubois et al. 2010; Hill et al. 2010; Glasel et al. 2011; Kasprian et al. 2011; Habas et al. 2012; Li et al. 2014; Leroy et al. 2015). Because the AF is more tightly organized on the left side, it may represent an early anatomical substrate for the leftward lateralization of the language network observed in the infant planum temporale during speech listening (Dehaene-Lambertz et al. 2002, 2010).

Asynchrony of Maturation Within the Language Network During Infancy

To detect differences in the maturational properties of bundles beyond their specific structural properties, the DTI parameters of infants were normalized to their adult reference (Dubois, Dehaene-Lambertz, Perrin, et al. 2008; Dubois, Dehaene-Lambertz, Soares, et al. 2008; Dubois, Dehaene-Lambertz, et al. 2014; Kulikova et al. 2014). In all analyses, transverse diffusivity was the most pertinent parameter to quantify the bundle myelination, which agrees with previous observations in infants (Dubois, Dehaene-Lambertz, Soares, et al. 2008) and animals (Song et al. 2002, 2005).

Asymmetries in the Bundle Maturation

The main differences in maturation between the left and right tracts were observed in the AF, SLF, and MLF, showing leftward asymmetries for normalized anisotropy (nFA) and one of the two normalized diffusivities ($n\lambda_{/\!/}$ or $n\lambda_{\perp}$). According to the hypotheses on the relationships between microstructural mechanisms and DTI parameters (see the "Individual measures of DTI parameters" section), this finding suggests that these asymmetries were related to differences in fiber coherence, bundle compactness, or amount of crossing fibers. Nevertheless, we could not exclude a difference in myelination for the MLF because of the lack of $n\lambda_{/\!/}$ asymmetry. These bundles may be more tightly organized in the left hemisphere than in the right at this age specifically, since these maturational asymmetries remained even after normalizing for microstructural asymmetries in the adult group. Because the AF and MLF project mostly above and to a lesser extent beyond the superior temporal sulcus, these bundle asymmetries may be related to maturational asymmetries in the cortex of the superior temporal sulcus and gyrus. Nevertheless, because a more mature cortex was detected in the right STS than in the left STS in infants (Leroy et al. 2011), further correlation studies between gray and white matter development in the same infants are needed to better understand the complementarity of these asymmetries within the language network. Other maturational asymmetries were detected in ventral bundles, but their meaning could not be clearly interpreted because of the lack of conjunctions between the different normalized DTI parameters.

Maturation of the Language Pathways

Finally, 3 classes of bundles with different patterns of maturation were distinguished in our study based on the 3 normalized DTI parameters and on $n\lambda_{\perp}$ only: (1) the AF and SLF were the least mature bundles; (2) the iFOF-EC fasciculus, the ILF, and its ILFlat branches showed intermediate maturation; (3) the MLF and UF were the most mature bundles. The analyses of normalized transverse diffusivity further detailed the maturational differences between the dorsal and ventral pathways: although the dorsal pathway was less mature than the ventral pathway, the dorsal progression was faster over this short developmental period. While Pujol et al. (2006) described a similar pattern of myelination in both the comprehension and production regions during the first 3 post-natal years, our results agree with 2 DTI studies which reported a delayed maturation of the dorsal bundles (Zhang et al. 2007; Brauer et al. 2013). Unlike some other bundles, the SLF matures slowly during childhood (Zhang et al. 2007).

Although a recent study also argued that the EC and iFOF were more mature than the AF in newborns (Perani et al. 2011; Brauer et al. 2013), the results that supported this conclusion were equivocal because structural differences between adult tracts were not taken into account. This asynchronous maturation between the dorsal and ventral pathways in infants also agrees with the phylogenetic development of bundles across species: the delayed maturation of the AF and SLF in infants may be related to their more recent evolution along the primate lineage (Rilling et al. 2008, 2012; Petrides and Pandya 2009).

The maturation asynchrony in the bundles of the language network should be compared with the maturation asynchrony across cortical regions connected by these pathways. Indeed, myelination significantly increases the conduction speed of the nerve impulse (Baumann and Pham-Dinh 2001) and is assumed to improve the functional efficiency of brain networks (van der Knaap et al. 1991). Conversely, neuronal activity induced by stimulation influences the degree of white matter myelination (Gyllensten and Malmfors 1963; Tauber et al. 1980; Barres and Raff 1993; Demerens et al. 1996). Recently, we detailed the maturation asynchrony of the infant linguistic network by distinguishing 3 classes of perisylvian cortical regions (Leroy et al. 2011): as expected, the most mature region was the primary auditory cortex (Heschl's gyrus), but the most immature class consisted of the superior temporal sulcus and the supramarginal gyrus, whereas the planum temporale and all inferior frontal sulci showed intermediate maturation. Here, we observed that the lag in maturation of the dorsal pathway was ultimately eliminated, which may be analogous to the convergence in maturity of the left superior temporal gyrus and supramarginal gyrus during the first postnatal weeks (Leroy et al. 2011). The correlation of maturation between the frontal region, the posterior STS, and the AF suggested a synchronized maturation within the dorsal pathway (Leroy et al. 2011). Future studies that include all linguistic bundles and gray matter parcels will help to delineate the respective roles of the dorsal and ventral pathways during language development. A potential perspective would be to detail the sequential dynamics of maturation across temporal and frontal regions by analyzing the direction of myelination along the AF and iFOF-EC, which both gather temporo-frontal and fronto-temporal fibers. Assuming that myelination proceeds from the neuron body to the periphery (McCart and Henry 1994), the fronts of maturation can be investigated based on the variations of DTI parameters along bundles, as proposed along the infant optic radiations (Dubois, Dehaene-Lambertz, Soares, et al. 2008) and along the AF in children learning to read (Yeatman et al. 2011).

Conclusion

Along with the structural development of brain networks, the infant's linguistic capacities dramatically increase during the first 2 years. Notably, infants progressively enhance their mainly auditory initial representations with new visual and motor inputs during the first months. This enhancement suggests an increase in information exchange across the auditory, visual, and motor regions, and the maturational convergence of the dorsal pathway may sustain this phenomenon because it is involved in sensory-motor integration. Future structural analyses that utilize correlations with functional imaging are expected to shed light on the crucial circuits that are required to develop a language system in humans.

Funding

This work was supported by the Fyssen Foundation, the "Fondation de France," the "Ecole des Neurosciences de Paris," the "Fondation Motrice," the McDonnell Foundation, and the French National Agency for Research (ANR). The finalization of this work received support from the European Union Seventh Framework Program (FP7/2007-2013, grant agreement no. 604102).

Notes

The authors thank the UNIACT clinical team for precious help in scanning the infants, and especially Gaëlle Mediouni. *Conflict of Interest*: None declared.

References

Axer H, Klingner CM, Prescher A. 2012. Fiber anatomy of dorsal and ventral language streams. Brain Lang. 127:192–204.

Barres BA, Raff MC. 1993. Proliferation of oligodendrocyte precursor cells depends on electrical activity in axons. Nature. 361:258–260.

Baumann N, Pham-Dinh D. 2001. Biology of oligodendrocyte and myelin in the mammalian central nervous system. Physiol Rev. 81:871–927.

Beaulieu C. 2002. The basis of anisotropic water diffusion in the nervous system—a technical review. NMR Biomed. 15:435–455.

Brauer J, Anwander A, Friederici AD. 2011. Neuroanatomical prerequisites for language functions in the maturing brain. Cereb Cortex. 21:459–466.

Brauer J, Anwander A, Perani D, Friederici AD. 2013. Dorsal and ventral pathways in language development. Brain Lang. 127:289–295.

Bristow D, Dehaene-Lambertz G, Mattout J, Soares C, Gliga T, Baillet S, Mangin JF. 2009. Hearing faces: how the infant brain matches the face it sees with the speech it hears. J Cogn Neurosci. 21:905–921.

Brody BA, Kinney HC, Kloman AS, Gilles FH. 1987. Sequence of central nervous system myelination in human infancy. I. An autopsy study of myelination. J Neuropathol Exp Neurol. 46:283–301.

Buchel C, Raedler T, Sommer M, Sach M, Weiller C, Koch MA. 2004. White matter asymmetry in the human brain: a diffusion tensor MRI study. Cereb Cortex. 14:945–951.

Catani M, Howard RJ, Pajevic S, Jones DK. 2002. Virtual in vivo interactive dissection of white matter fasciculi in the human brain. Neuroimage. 17:77–94.

Catani M, Mesulam M. 2008. The arcuate fasciculus and the disconnection theme in language and aphasia: history and current state. Cortex. 44: 53–961.

Catani M, Thiebaut de Schotten M. 2008. A diffusion tensor imaging tractography atlas for virtual in vivo dissections. Cortex. 44:1105–1132.

Chi JG, Dooling EC, Gilles FH. 1977. Left-right asymmetries of the temporal speech areas of the human fetus. Arch Neurol. 34:346–348.

David O, Job AS, De Palma L, Hoffmann D, Minotti L, Kahane P. 2013. Probabilistic functional tractography of the human cortex. Neuroimage. 80:307–317.

de Boysson-Bardies B, Vihman MM. 1991. Adaptation to language: evidence from babbling and first words in four languages. Language. 67:297–319.

Dehaene-Lambertz G, Dehaene S, Anton JL, Campagne A, Ciuciu P, Dehaene GP, Denghien I, Jobert A, Lebihan D, Sigman M, et al. 2006. Functional segregation of cortical language areas by sentence repetition. Hum Brain Mapp. 27:360–371.

Dehaene-Lambertz G, Dehaene S, Hertz-Pannier L. 2002. Functional neuroimaging of speech perception in infants. Science. 298:2013–2015.

Dehaene-Lambertz G, Hertz-Pannier L, Dubois J, Meriaux S, Roche A, Sigman M, Dehaene S. 2006. Functional organization of perisylvian activation during presentation of sentences in preverbal infants. Proc Natl Acad Sci USA. 103:14240–14245.

Dehaene-Lambertz G, Montavont A, Jobert A, Allirol L, Dubois J, Hertz-Pannier L, Dehaene S. 2010. Language or music, mother or Mozart? Structural and environmental influences on infants' language networks. Brain Lang. 114:53–65.

Demerens C, Stankoff B, Logak M, Anglade P, Allinquant B, Couraud F, Zalc B, Lubetzki C. 1996. Induction of myelination in the central nervous system by electrical activity. Proc Natl Acad Sci USA. 93:9887–9892.

Descoteaux M, Angelino E, Fitzgibbons S, Deriche R. 2007. Regularized, fast, and robust analytical Q-ball imaging. Magn Reson Med. 58:497–510.

Dick AS, Tremblay P. 2012. Beyond the arcuate fasciculus: consensus and controversy in the connectional anatomy of language. Brain. 135:3529–3550.

Dubois J, Benders M, Cachia A, Lazeyras F, Ha-Vinh Leuchter R, Sizonenko SV, Borradori-Tolsa C, Mangin JF, Huppi PS. 2008. Mapping the early cortical folding process in the preterm newborn brain. Cereb Cortex. 18:1444–1454.

Dubois J, Benders M, Lazeyras F, Borradori-Tolsa C, Leuchter RH, Mangin JF, Huppi PS. 2010. Structural asymmetries of perisylvian regions in the preterm newborn. Neuroimage. 52:32–42.

Dubois J, Dehaene-Lambertz G, Kulikova S, Poupon C, Hüppi PS, Hertz-Pannier L. 2014. The early development of brain white matter: a review of imaging studies in fetuses, newborns and infants. Neuroscience. 276:48–71.

Dubois J, Dehaene-Lambertz G, Perrin M, Mangin JF, Cointepas Y, Duchesnay E, Le Bihan D, Hertz-Pannier L. 2008. Asynchrony of the early maturation of white matter bundles in healthy infants: quantitative landmarks revealed noninvasively by diffusion tensor imaging. Hum Brain Mapp. 29:14–27.

Dubois J, Dehaene-Lambertz G, Soares C, Cointepas Y, Le Bihan D, Hertz-Pannier L. 2008. Microstructural correlates of infant functional development: example of the visual pathways. J Neurosci. 28:1943–1948.

Dubois J, Hertz-Pannier L, Cachia A, Mangin JF, Le Bihan D, Dehaene-Lambertz G. 2009. Structural asymmetries in the infant language and sensori-motor networks. Cereb Cortex. 19:414–423.

Dubois J, Hertz-Pannier L, Dehaene-Lambertz G, Cointepas Y, Le Bihan D. 2006. Assessment of the early organization and maturation of infants' cerebral white matter fiber bundles: a feasibility study using quantitative diffusion tensor imaging and tractography. Neuroimage. 30:1121–1132.

Dubois J, Kostovic I, Judas M. 2015. Development of structural and functional connectivity. In: Toga AW, editor. Brain mapping: an encyclopedic reference, vol. 2, pp. 423–437. Academic Press: Elsevier.

Dubois J, Kulikova S, Hertz-Pannier L, Mangin JF, Dehaene-Lambertz G, Poupon C. 2014. Correction strategy for diffusion-weighted images corrupted with motion: application to the DTI evaluation of infants' white matter. Magn Reson Imaging. 32:981–992.

Duclap D, Schmitt B, Lebois A, Riff O, Guevara P, Marrakchi-Kacem L, Brion V, Poupon F, Mangin JF, Poupon C. 2012. Connectomist-2.0: a novel diffusion analysis toolbox for BrainVISA. In: Proceedings of the 29th ESMRMB meeting: 842. Lisbon, Portugal, 4–6 October 2012.

Feinberg DA, Moeller S, Smith SM, Auerbach E, Ramanna S, Gunther M, Glasser MF, Miller KL, Ugurbil K, Yacoub E. 2010. Multiplexed echo planar imaging for sub-second whole brain FMRI and fast diffusion imaging. PLoS ONE. 5:e15710.

Flechsig P. 1920. Anatomie des Menschlichen Gehirn und Rückenmarks, auf myelogenetischer grundlage. Leipzig: G. Thieme.

Forkel SJ, Thiebaut de Schotten M, Kawadler JM, Dell'acqua F, Danek A, Catani M. 2014. The anatomy of fronto-occipital connections from early blunt dissections to contemporary tractography. Cortex. 56:73–84.

Frey S, Campbell JS, Pike GB, Petrides M. 2008. Dissociating the human language pathways with high angular resolution diffusion fiber tractography. J Neurosci. 28:11435–11444.

Friederici AD, Mueller JL, Oberecker R. 2011. Precursors to natural grammar learning: preliminary evidence from 4-month-old infants. PLoS ONE. 6:e17920.

Glasel H, Leroy F, Dubois J, Hertz-Pannier L, Mangin JF, Dehaene-Lambertz G. 2011. A robust cerebral asymmetry in the infant brain: the rightward superior temporal sulcus. Neuroimage. 58:716–723.

Gyllensten L, Malmfors T. 1963. Myelinization of the optic nerve and its dependence on visual function—a quantitative investigation in mice. J Embryol Exp Morphol. 11:255–266.

Habas PA, Scott JA, Roosta A, Rajagopalan V, Kim K, Rousseau F, Barkovich AJ, Glenn OA, Studholme C. 2012. Early folding patterns and asymmetries of the normal human brain detected from in utero MRI. Cereb Cortex. 22:13–25.

Hickok G, Poeppel D. 2007. The cortical organization of speech processing. Nat Rev Neurosci. 8:393–402.

Hill J, Dierker D, Neil J, Inder T, Knutsen A, Harwell J, Coalson T, Van Essen D. 2010. A surface-based analysis of hemispheric asymmetries and folding of cerebral cortex in term-born human infants. J Neurosci. 30:2268–2276.

Huang H, Zhang J, van Zijl PC, Mori S. 2004. Analysis of noise effects on DTI-based tractography using the brute-force and multi-ROI approach. Magn Reson Med. 52:559–565.

Huang H, Zhang J, Wakana S, Zhang W, Ren T, Richards LJ, Yarowsky P, Donohue P, Graham E, van Zijl PC, et al. 2006. White and gray matter development in human fetal, newborn and pediatric brains. Neuroimage. 33:27–38.

Johnson EK, Tyler MD. 2010. Testing the limits of statistical learning for word segmentation. Dev Sci. 13:339–345.

Jusczyk PW. 1997. The discovery of spoken language. Cambridge (MA): MIT Press.

Kasprian G, Langs G, Brugger PC, Bittner M, Weber M, Arantes M, Prayer D. 2011. The prenatal origin of hemispheric asymmetry: an in utero neuroimaging study. Cereb Cortex. 21:1076–1083.

Kinney HC, Brody BA, Kloman AS, Gilles FH. 1988. Sequence of central nervous system myelination in human infancy. II. Patterns of myelination in autopsied infants. J Neuropathol Exp Neurol. 47:217–234.

Kostovic I, Jovanov-Milosevic N, Rados M, Sedmak G, Benjak V, Kostovic-Srzentic M, Vasung L, Culjat M, Huppi P, Judas M. 2014. Perinatal and early postnatal reorganization of the subplate and related cellular compartments in the human cerebral wall as revealed by histological and MRI approaches. Brain Struct Funct. 219:231–253.

Kostovic I, Rakic P. 1990. Developmental history of the transient subplate zone in the visual and somatosensory cortex of the macaque monkey and human brain. J Comp Neurol. 297:441–470.

Kuhl PK, Meltzoff AN. 1982. The bimodal perception of speech in infancy. Science. 218:1138–1141.

Kuhl PK, Meltzoff AN. 1996. Infant vocalizations in response to speech: vocal imitation and developmental change. J Acoust Soc Am. 100:2425–2438.

Kulikova S, Hertz-Pannier L, Dehaene-Lambertz G, Buzmakov A, Poupon C, Dubois J. 2014. Multi-parametric evaluation of the white matter maturation. Brain Struct Funct. Pubmed PMID: 25183543.

LaMantia AS, Rakic P. 1990. Axon overproduction and elimination in the corpus callosum of the developing rhesus monkey. J Neurosci. 10:2156–2175.

LaMantia AS, Rakic P. 1994. Axon overproduction and elimination in the anterior commissure of the developing rhesus monkey. J Comp Neurol. 340:328–336.

Lazar M, Weinstein DM, Tsuruda JS, Hasan KM, Arfanakis K, Meyerand ME, Badie B, Rowley HA, Haughton V, Field A, et al. 2003. White matter tractography using diffusion tensor deflection. Hum Brain Mapp. 18:306–321.

Leroy F, Glasel H, Dubois J, Hertz-Pannier L, Thirion B, Mangin JF, Dehaene-Lambertz G. 2011. Early maturation of the linguistic dorsal pathway in human infants. J Neurosci. 31: 1500–1506.

Leroy F, Cai Q, Bogart SL, Dubois J, Coulon O, Monzalvo K, Fischer C, Glasel H, Van der Haegen L, Bénézit A, et al. 2015. New human-specific brain landmark: the depth asymmetry of superior temporal sulcus. Proc Natl Acad Sci USA. 112(4): 1208–1213.

Li G, Nie J, Wang L, Shi F, Lyall AE, Lin W, Gilmore JH, Shen D. 2014. Mapping longitudinal hemispheric structural asymmetries of the human cerebral cortex from birth to 2 years of age. Cereb Cortex. 24:1289–1300.

Liu Y, Baleriaux D, Kavec M, Metens T, Absil J, Denolin V, Pardou A, Avni F, Van Bogaert P, Aeby A. 2010. Structural asymmetries in motor and language networks in a population of healthy preterm neonates at term equivalent age: a diffusion tensor imaging and probabilistic tractography study. Neuroimage. 51:783–788.

Mahmoudzadeh M, Dehaene-Lambertz G, Fournier M, Kongolo G, Goudjil S, Dubois J, Grebe R, Wallois F. 2013. Syllabic discrimination in premature human infants prior to complete formation of cortical layers. Proc Natl Acad Sci USA. 110:4846–4851.

Makris N, Pandya DN. 2009. The extreme capsule in humans and rethinking of the language circuitry. Brain Struct Funct. 213:343–358.

Martino J, Brogna C, Robles SG, Vergani F, Duffau H. 2010. Anatomic dissection of the inferior fronto-occipital fasciculus revisited in the lights of brain stimulation data. Cortex. 46:691–699.

Matsumoto R, Nair DR, LaPresto E, Najm I, Bingaman W, Shibasaki H, Luders HO. 2004. Functional connectivity in the human language system: a cortico-cortical evoked potential study. Brain. 127:2316–2330.

McCart RJ, Henry GH. 1994. Visual corticogeniculate projections in the cat. Brain Res. 653:351–356.

Moeller S, Yacoub E, Olman CA, Auerbach E, Strupp J, Harel N, Ugurbil K. 2010. Multiband multislice GE-EPI at 7 tesla, with 16-fold acceleration using partial parallel imaging with application to high spatial and temporal whole-brain fMRI. Magn Reson Med. 63:1144–1153.

Nossin-Manor R, Card D, Morris D, Noormohamed S, Shroff MM, Whyte HE, Taylor MJ, Sled JG. 2013. Quantitative MRI in the very preterm brain: assessing tissue organization and myelination using magnetization transfer, diffusion tensor and T(1) imaging. Neuroimage. 64:505–516.

Pallier C, Devauchelle AD, Dehaene S. 2011. Cortical representation of the constituent structure of sentences. Proc Natl Acad Sci USA. 108:2522–2527.

Parker GJ, Luzzi S, Alexander DC, Wheeler-Kingshott CA, Ciccarelli O, Lambon Ralph MA. 2005. Lateralization of ventral and dorsal auditory-language pathways in the human brain. Neuroimage. 24:656–666.

Perani D, Saccuman MC, Scifo P, Anwander A, Spada D, Baldoli C, Poloniato A, Lohmann G, Friederici AD. 2011. Neural language networks at birth. Proc Natl Acad Sci USA. 108:16056–16061.

Perrin M, Poupon C, Cointepas Y, Rieul B, Golestani N, Pallier C, Riviere D, Constantinesco A, Le Bihan D, Mangin JF. 2005. Fiber tracking in q-ball fields using regularized particle trajectories. Inf Process Med Imaging. 19:52–63.

Petanjek Z, Judas M, Simic G, Rasin MR, Uylings HB, Rakic P, Kostovic I. 2011. Extraordinary neoteny of synaptic spines in the human prefrontal cortex. Proc Natl Acad Sci USA. 108:13281–13286.

Petersson KM, Folia V, Hagoort P. 2012. What artificial grammar learning reveals about the neurobiology of syntax. Brain Lang. 120:83–95.

Petrides M, Pandya DN. 2009. Distinct parietal and temporal pathways to the homologues of Broca's area in the monkey. PLoS Biol. 7:e1000170.

Price CJ. 2010. The anatomy of language: a review of 100 fMRI studies published in 2009. Ann N Y Acad Sci. 1191:62–88.

Pujol J, Soriano-Mas C, Ortiz H, Sebastian-Galles N, Losilla JM, Deus J. 2006. Myelination of language-related areas in the developing brain. Neurology. 66:339–343.

Rakic P, Riley KP. 1983. Overproduction and elimination of retinal axons in the fetal rhesus monkey. Science. 219:1441–1444.

Rauschecker JP, Scott SK. 2009. Maps and streams in the auditory cortex: nonhuman primates illuminate human speech processing. Nat Neurosci. 12:718–724.

Rilling JK, Glasser MF, Jbabdi S, Andersson J, Preuss TM. 2012. Continuity, divergence, and the evolution of brain language pathways. Front Evol Neurosci. 3:11.

Rilling JK, Glasser MF, Preuss TM, Ma X, Zhao T, Hu X, Behrens TE. 2008. The evolution of the arcuate fasciculus revealed with comparative DTI. Nat Neurosci. 11:426–428.

Riviere D, Papadopoulos-Orfanos D, Poupon C, Poupon F, Coulon O, Poline JB, Frouin V, Regis J, M JF. 2000. A structural browser for human brain mapping. In: Proceedings of the 6th HBM Scientific Meeting, San Antonio, USA. NeuroImage. 11:S912.

Rolheiser T, Stamatakis EA, Tyler LK. 2011. Dynamic processing in the human language system: synergy between the arcuate fascicle and extreme capsule. J Neurosci. 31:16949–16957.

Saur D, Kreher BW, Schnell S, Kummerer D, Kellmeyer P, Vry MS, Umarova R, Musso M, Glauche V, Abel S, et al. 2008. Ventral and dorsal pathways for language. Proc Natl Acad Sci USA. 105:18035–18040.

Seabold JS, Perktold J. 2010. Statsmodels: econometric and statistical modeling with python. In: Proceedings of the 9th Python in Science Conference. 2010 Jun 28–July 3; USA: Austin. P57.

Song JW, Mitchell PD, Kolasinski J, Ellen Grant P, Galaburda AM, Takahashi E. 2014. Asymmetry of white matter pathways in developing human brains. Cereb Cortex. Pubmed PMID: 24812082.

Song SK, Sun SW, Ramsbottom MJ, Chang C, Russell J, Cross AH. 2002. Dysmyelination revealed through MRI as increased radial (but unchanged axial. Diffusion of water. Neuroimage. 17:1429–1436.

Song SK, Yoshino J, Le TQ, Lin SJ, Sun SW, Cross AH, Armstrong RC. 2005. Demyelination increases radial diffusivity in corpus callosum of mouse brain. Neuroimage. 26:132–140.

Takahashi E, Folkerth RD, Galaburda AM, Grant PE. 2012. Emerging cerebral connectivity in the human fetal brain: an MR tractography study. Cereb Cortex. 22:455–464.

Tauber H, Waehneldt TV, Neuhoff V. 1980. Myelination in rabbit optic nerves is accelerated by artificial eye opening. Neurosci Lett. 16:235–238.

Thiebaut de Schotten M, Cohen L, Amemiya E, Braga L, Dehaene S. 2012. Learning to read improves the structure of the arcuate fasciculus. Cereb Cortex. 24:989–995.

Thiebaut de Schotten M, Dell'Acqua F, Forkel SJ, Simmons A, Vergani F, Murphy DG, Catani M. 2011. A lateralized brain network for visuospatial attention. Nat Neurosci. 14:1245–1246.

Thiebaut de Schotten M, Ffytche DH, Bizzi A, Dell'Acqua F, Allin M, Walshe M, Murray R, Williams SC, Murphy DG, Catani M. 2011. Atlasing location, asymmetry and inter-subject variability of white matter tracts in the human brain with MR diffusion tractography. Neuroimage. 54:49–59.

Turken AU, Dronkers NF. 2011. The neural architecture of the language comprehension network: converging evidence from lesion and connectivity analyses. Front Syst Neurosci. 5:1.

van der Knaap MS, Valk J, Bakker CJ, Schooneveld M, Faber JA, Willemse J, Gooskens RH. 1991. Myelination as an expression of the functional maturity of the brain. Dev Med Child Neurol. 33:849–857.

Vandermosten M, Boets B, Poelmans H, Sunaert S, Wouters J, Ghesquiere P. 2012. A tractography study in dyslexia: neuroanatomic correlates of orthographic, phonological and speech processing. Brain. 135:935–948.

Vasung L, Huang H, Jovanov-Milosevic N, Pletikos M, Mori S, Kostovic I. 2010. Development of axonal pathways in the human fetal fronto-limbic brain: histochemical characterization and diffusion tensor imaging. J Anat. 217:400–417.

Witelson SF, Pallie W. 1973. Left hemisphere specialization for language in the newborn. Neuroanatomical evidence of asymmetry. Brain. 96:641–646.

Wong FC, Chandrasekaran B, Garibaldi K, Wong PC. 2011. White matter anisotropy in the ventral language pathway predicts sound-to-word learning success. J Neurosci. 31:8780–8785.

Xing D, Papadakis NG, Huang CL, Lee VM, Carpenter TA, Hall LD. 1997. Optimised diffusion-weighting for measurement of apparent diffusion coefficient (ADC) in human brain. Magn Reson Imaging. 15:771–784.

Yakovlev PI, Lecours AR. 1967. The myelogenetic cycles of regional maturation in the brain. In: Minowski A, editors. Regional development of the brain in early life. Oxford: Blackwell. p. 3–69.

Yeatman JD, Dougherty RF, Rykhlevskaia E, Sherbondy AJ, Deutsch GK, Wandell BA, Ben-Shachar M. 2011. Anatomical properties of the arcuate fasciculus predict phonological and reading skills in children. J Cogn Neurosci. 23:3304–3317.

Zanin E, Ranjeva JP, Confort-Gouny S, Guye M, Denis D, Cozzone PJ, Girard N. 2011. White matter maturation of normal human fetal brain. An in vivo diffusion tensor tractography study. Brain Behav. 1:95–108.

Zhang J, Evans A, Hermoye L, Lee SK, Wakana S, Zhang W, Donohue P, Miller MI, Huang H, Wang X, et al. 2007. Evidence of slow maturation of the superior longitudinal fasciculus in early childhood by diffusion tensor imaging. Neuroimage. 38:239–247.